A NEW EFFICIENCY MODEL FOR A REGENERATIVE DYNAMOMETER

Mark Croft Geoffrey Walker Geir Hovland

School of ITEE
University of Queensland
Brisbane, Australia
Email: {mcroft, walkerg, hovland}@itee.uq.edu.au
Fax: +61 7 3365 4999

Abstract
This paper presents two efficiency models for the regenerative dynamometer to be built at the University of Queensland. The models incorporate an accurate accounting of the losses associated with the regenerative dynamometer and the battery modelling technique used. In addition to the models the cycle and instantaneous efficiencies were defined for a regenerative system that requires a desired torque output. The simulation of the models allowed the instantaneous and cycle efficiencies to be examined. The results show the intended dynamometer machine has significant efficiency draw backs but incorporating field winding control, the efficiency can be improved.

1 INTRODUCTION

The push for environmentally responsible technologies has seen a greater emphasis put on reduced vehicle fuel consumption and emissions. Consequently many car manufactures have developed hybrid-electric vehicles such as the Toyota Prius and Honda Insight. The Sustainable Energy Research Group (SERG) at the University of Queensland is currently developing a hybrid-electric vehicle called the Ultracommuter [1] .

The drive train to be implemented in the Ultracommuter consists of two wheel motors and a range extender (topology still to be decided). The wheel motors topology is an ironless brushless DC motor (BLDC motor) [2]. These motors are characterised by very low spinning (no load) losses, yet very high peak torque capability limited only by the thermal limitations of the copper windings and their associated potted structure. The efficiency of the motors is high over a large part of their torque-speed map, and notably in the region where they will spend most of their time in typical operation [2, 3].

As part of the development of the Ultracommuter a motor test platform is to be constructed. The conventional use of a motor test platform is to deliver a constant torque so that efficiency mapping can be completed and burst loading to measure peak performance and thermal characteristics. To effectively and accurately test the true energy consumption under dynamic operation an electric vehicle drive train test platform must be capable of emulating the opposing forces produced on the vehicle under driving conditions.

This paper presents two models for a regenerative dynamometer. These models incorporate an accurate accounting for all the loss mechanisms within the regenerative dynamometer. This allows the cycle and instantaneous efficiencies for the dynamometer to be calculated and determination if grid connectivity is possible.

2 DYNAMOMETER REQUIREMENTS

The key component of the test platform, the dynamometer, must be capable of accurately producing the required load torque, controlling the rapidly changing torques involved in simulating road conditions and allow bidirectional torque control. Hence conventional water, frictional or eddy-current brake dynamometers lack the dynamic response, controllability and precision to accurately emulate the road load, therefore an electric motor/generator is the ideal machine for use as the dynamometer.

The regeneration characteristics of an electric motor have been incorporated in the dynamometer design primarily because of control reasons. The advantages of regeneration become obvious at the high speeds and high torques used for burst testing. This will require up to 50kW to be absorbed by the dynamometer. In addition the motor under test (MUT) will require up to 50kW to be delivered by the power source. Regeneration allows the power recovered from the dynamometer to be recirculated to power the MUT. This has two advantages. The first is to reduce the size of the power electronics (grid connection) or reduce the energy storage requirements of the power source (batteries). The second advantage is the elimination of a power dissipation system for the energy generated from the dynamometer. The drawback of this approach is that expensive power electronics need to be implemented for the regenerative dynamometer topology.

m	Mass of the vehicle
a	Acceleration of the vehicle
ρ	Density of air
C_D	Coefficient of drag
A	Frontal area of the vehicle
v	Velocity of the vehicle
C_{RR}	Coefficient of rolling resistance
θ_r	Angle of the road relative to gravitational force
$\dot{\theta}$	Angular velocity
$\ddot{\theta}$	Angular acceleration
r	Radius of the vehicle's tyre
J_{Dyno}, B_{Dyno}, $\dot{\theta}_{Dyno}$ and $\ddot{\theta}_{Dyno}$	Inertia, Viscous friction coefficient, angular velocity and angular acceleration for the dynamometer
J_{MUT}, B_{MUT}, $\dot{\theta}_{MUT}$ and $\ddot{\theta}_{MUT}$	Inertia, Viscous friction coefficient, angular velocity and angular acceleration for the MUT
$\dot{\theta}_{rotor}$	Angular velocity of the rotor
$\ddot{\theta}_{rotor}$	Angular acceleration of the rotor
$\ddot{\theta}_{ref}$, $\dot{\theta}_{ref}$ and θ_{ref}	Angular acceleration, angular velocity and angular position reference value.
J_{rotor}	The combined inertia of the Dynamometer and the MUT
P	Proportional Gain
I	Integral Gain
D	Damper size of the coupling
K	Spring size of the coupling
R	Radius of the armature
l	Length of the armature
p_{pairs}	Number of pole pairs in the motor
K_h	Coefficient of hysteresis loss
K_e	Coefficient of eddy current loss
B	Flux density
n	Steinmetz component
I	Instantaneous armature current
R_{Dyno}	Dynamometer armature resistance
V_{brush}	Voltage drop across the brushes
V_{bus}	Bus voltage of the Dynamometer
fs	Switching frequency
$Duty$	Duty ratio for the power electronics
E_o	Fully charged battery terminal voltage
R_o	Fully charged battery terminal resistance
f	State of charge

Table 1: Nomenclature

3 MODELING THE REGENRATIVE DYNAMOMETER

To simulate the opposing forces produced on the vehicle under driving the linear force produced at the connection of the rear tyres and road is given by

$$F_{road} = ma + \frac{1}{2}\rho C_D A v^2 + C_{RR} mg + mg\sin\theta_r \qquad (1)$$

This force is translated into the rotational system of the tyre, wheel and motor. The equivalent torque is given in Eqn (2) [4].

$$T_{road} = m\ddot{\theta} r^2 + \frac{1}{2}\rho C_D A \dot{\theta}^2 r^3 + C_{RR} mgr + mgr\sin\theta_r \qquad (2)$$

3.1 Rigid Mass Model

The rigid mass model was developed first because the dynamometer output shaft flange will be rigidly coupled to the MUT rotor [5]. The system can be modelled as a single shaft with the electromechanical torque produced by the dynamometer acting on one end of the shaft and the electromechanical torque produced by the MUT acting on the other end. Figure 1 shows the mechanical representation of the rigid mass model.

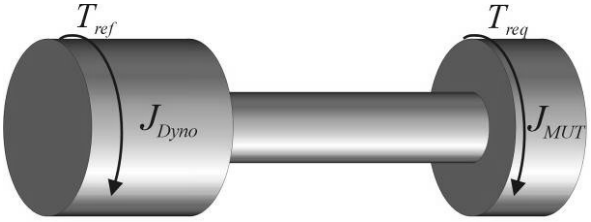

Figure 1: Rigid mass model.

The angular acceleration of the rigid mass system is defined by Eqn (3) assuming the coulomb friction of the shaft bearings of the dynamometer and MUT is negligible.

$$\ddot{\theta}_{Rotor} = \frac{T_{Req} - T_{ref} - \left(B_{Dyno} + B_{MUT}\right)\dot{\theta}_{rotor}}{J_{rotor}} \qquad (3)$$

Where the MUT speed control loop sets the desired electromechanical torque, T_{Req} to

$$T_{Req} = P\left(\dot{\theta}_{ref} - \dot{\theta}_{rotor}\right) + I\left(\theta_{ref} - \theta_{rotor}\right) \qquad (4)$$

And T_{ref} is the electromechanical torque required by the Dynamometer to simulate the road conditions.

$$T_{ref} = \frac{1}{2}\left(\begin{array}{l} m\ddot{\theta}_{ref} r^2 + \frac{1}{2}\rho C_D A \dot{\theta}_{ref}^2 r^3 + C_{RR} mgr \\ + mgr\sin\theta_r - J_{Dyno}\ddot{\theta}_{ref} - B_{Dyno}\dot{\theta}_{ref} \end{array}\right) \qquad (5)$$

3.2 Spring-damper Model

The spring-damper model was developed primarily because the rigid mass model didn't simulate the interaction of the tyre on the road. Under high torques and high loading the tyre undergoes elastic deformation; this phenomenon can be simply modelled as a spring and damper connection between the tyre rim and the road. The rigid connection between the Dynamometer and MUT in the previous model was changed to a spring-damper connection allowing the dynamics of the tyre on the road to be simulated. Figure 2 is the mechanical representation of the spring damper model.

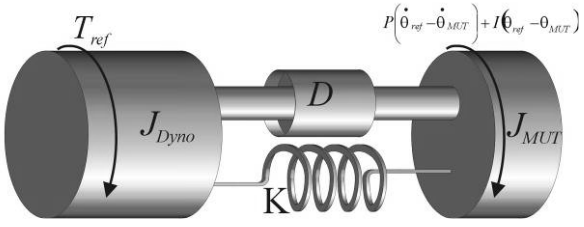

Figure 2: Spring-damper model.

The system can be defined by the separate angular accelerations of the dynamometer and MUT.

$$\ddot{\theta}_{Dyno} = \frac{T_{ref} + T_{SD} - B_{Dyno}\dot{\theta}_{Dyno}}{J_{Dyno}} \quad (6)$$

$$\ddot{\theta}_{MUT} = \frac{P\left(\dot{\theta}_{ref} - \dot{\theta}_{MUT}\right) + I\left(\theta_{ref} - \theta_{MUT}\right) - T_{SD} - B_{MUT}\dot{\theta}_{MUT}}{J_{MUT}} \quad (7)$$

Where T_{SD} is the torque produce across the spring-damper connection and is specified by Eqn (8).

$$T_{SD} = D\left(\dot{\theta}_{MUT} - \dot{\theta}_{Dyno}\right) + K\left(\theta_{MUT} - \theta_{Dyno}\right) \quad (8)$$

3.3 Power losses

There are three categories of power loss in a separately excited DC regenerative dynamometer: mechanical losses, electrical losses and power electronic losses.

3.3.1 Mechanical losses

There are four mechanical loss mechanisms in the regenerative dynamometer.

3.3.1.1 Windage Loss

The windage of an electric machine can be calculated for Eqn (9) [6].

$$P_{windage} = \pi C_d \rho R^4 \dot{\theta}^3 l \quad \text{W} \quad (9)$$

Where C_d is the skin-friction coefficient for the armature of the regenerative dynamometer and is given by

$$2.04 = \frac{1}{\sqrt{C_d}} - 1.768\ln(\mathrm{Re}\sqrt{C_d}) \quad (10)$$

The Reynolds Number, Re, should be greater than 2000 because is assumed the air gap in the dynamometer experiences turbulent flow [6, 7].

3.3.1.2 Brush and Bearing Loss

Brush and bearing loss is best quantified experimentally as brush configuration and bearings vary from machine to machine and loss may vary significantly. A run-down test was performed on the dynamometer with brushes lowered and bedded in [8]. The power loss associated with the bearing and brush friction was approximated by a first order equation, Eqn (11), to give the coulomb and viscous friction coefficients for this regenerative dynamometer.

$$P_{bearing+brush} = 0.0115\dot{\theta} + 0.93 \ \text{W} \quad (11)$$

3.3.1.3 Hysteresis and Eddy Current Loss

Hysteresis losses can be calculated from

$$P_{hysteresis} = \frac{p_{pairs}}{2\pi} K_h \dot{\theta} B^n \quad \text{W} \quad (12)$$

And eddy current losses can be calculated from [9]

$$P_{eddy} = \left(\frac{p_{pairs}}{2\pi}\right)^2 K_e \dot{\theta}^2 B^2 \quad \text{W} \quad (13)$$

The power loss attributed to magnetic losses can be calculated only if the construction and materials of the DC machine is known. If the construction or the materials is unknown an alternate approach is to experimentally extract the value of the losses. This is easily achieved in a separately excited DC machine by completing run-down tests with the field windings energised and then with the field windings de-energised [8]. Then the resultant retarding torque attributed to the magnetic losses is the difference of the two run-down tests. Then Eqn (14) was fitted to the data using Matlab.

$$P_{magnetic} = 0.015905\dot{\theta} + 0.254667Log(2040.2194\dot{\theta}) \quad (14)$$

3.3.1.4 Stray Loss

Stray losses are generally incorporated to account for the increased magnetic losses caused by the changes in flux distribution due to the armature reaction field. The loss is generally assigned up to 1% of output power, for this case 0.67% is assigned for stray loss as the stator has been rewound to reduce this effect[8].

3.3.2 Electrical Losses

There are three electrical loss mechanisms in the regenerative dynamometer. The loss mechanisms are copper loss, brush loss and field loss and are given in Eqn (15), (16) and (17) respectively [6].

$$P_{winding} = i^2 R_{dyno} \ \text{W} \quad (15)$$

$$P_{Brush} = V_{brush} i \ \text{W} \quad (16)$$

$$P_{Field} = \frac{V_{Field}^2}{R_{Field}} \ \text{W} \quad (17)$$

3.3.3 Power Electronic losses

The power electronics topology for the regenerative dynamometer will utilize the Powerex Intellimod™ Module PM300RSD060. The PM300RSD060 is an integrated pack combining 3 IGBT half bridges with integrated gate drive circuitry. The pack also incorporates short circuit protection, over current protection and thermal shutdown [10].

There are two types of losses associated with this type of controller: switching and on-state losses

3.3.3.1 Switching Loss

The dynamometer will utilize two of the PM300RSD060 IGBT half-bridges in the armature circuit. A unipolar switching scheme will be implemented at the switching frequency of 15 kHz. The switching loss characteristics in the manufacturer's data are given at 300V. The manufacturer's data also plots the energy loss for each IGBT turn on and off. Linear regression lines were

applied to the data, hence the power loss associated with armature switching circuit is

$$P_{switching} = \frac{V_{bus}}{300}\left(7.22\times10^{-5}|i| - 4.21\times10^{-4}\right)\times fs \text{ W} \quad (18)$$

3.3.3.2 On-state Loss

The saturation voltage and diode forward voltage drop characteristics of the PM300RDS060 are also given in the manufacturer's data. Linear regression lines were fitted to the manufacturer's data and the saturation voltage and diode forward voltage drop was determined to be

$$V_{saturation} = 1.66\times10^{-3} i + 1.125 \quad \text{V} \quad (19)$$

$$V_{diode} = 3.9\times10^{-3} i + 1 \quad \text{V} \quad (20)$$

Hence the on-state losses associated with the armature full bridge circuit (unipolar switching) are defined as

$$P_{onstate} = (1 + Duty)\left(1.66\times10^{-3} i^2 + 1.125|i|\right) + (1 - \text{Duty})\left(3.9\times10^{-3} i^2 + |i|\right) \text{ W} \quad (21)$$

3.4 Comparison of Losses

The previously presented power losses in section 3.3 do not easily convey their corresponding magnitudes, hence are not easily visualised and compared as equations. All losses can be seen to be a function of either angular velocity (or voltage) or torque (or current) with the exception of stray loss and on-state losses. For completeness the on-state losses have been given at 15% duty ratio as this expected average duty ratio. The speed dependent losses have been presented in figure 3 and torque dependent losses have been presented in figure 4.

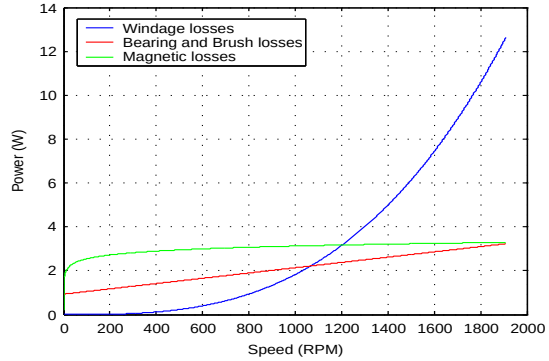

Figure 3: Speed dependent power losses.

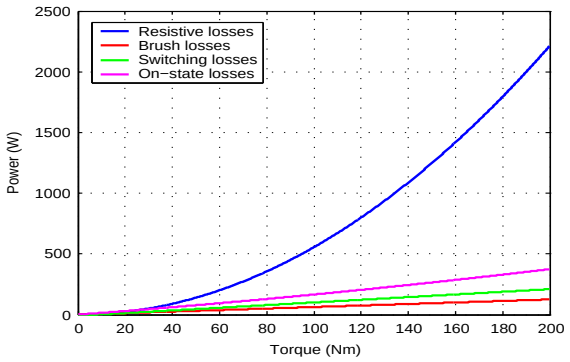

Figure 4: Torque dependent power losses.

3.5 Battery Pack

The battery pack anticipated for use as the buffer between the grid and the dynamometer is a series string of Hawker Genesis batteries. These batteries are 12V absorbed glass matt (AGM) lead-acid batteries and have been modelled using the Unnewehr universal model because of the dynamic nature of the current discharge/charge. The terminal voltage per battery is

$$E_{Terminal} = E_{oc} - Ri \quad (22)$$

Where E_{oc} is the no-load voltage and R is the internal resistance of the battery pack and given by Eqns (23) and (24) respectively.

$$E_{oc} = E_o - Kif \quad (23)$$

$$R = R_o - Krf \quad (24)$$

Ki and *Kr* are experimentally determined coefficients that compensate for the effect state of charge has on the terminal voltage and internal resistance[11, 12].

The battery pack current and voltage for a given power, P, is given by Eqn (25) and (26) respectively, assuming power being drawn from the battery pack is positive [11].

$$i_{Battery} = \left(E_{oc} - \sqrt{E_{oc}^2 - 4RP}\right)/2R \quad (25)$$

$$v_{Battery} = \left(E_{oc} + \sqrt{E_{oc}^2 - 4RP}\right)/2 \quad (26)$$

4 EFFICIENCY

There are two types of efficiency that can be defined for the regenerative dynamometer: cycle efficiency and instantaneous efficiency. Cycle efficiency is the efficiency over a given drive cycle and is defined as

$$\eta_{cycle} = \int |P_{out}| \Big/ \int |P_{in}| \quad (27)$$

And the instantaneous efficiency is defined as

$$\eta_{Instantaneous} = P_{out} / P_{in} \quad (28)$$

The critical component for calculating the efficiency for the regenerative dynamometer is defining the power out of the dynamometer, P_{out} and power into the dynamometer, P_{in} correctly. A motor under normal operating conditions has electrical power flowing in and mechanical power flowing out. When the motor is operated as a generator the power flows are reversed.

The power flows in a regenerative dynamometer are more complex. Given that instantaneously both the electrical power flow and mechanical power flow can take either sign, there are four combinations of power flows that might occur in the regenerative dynamometer. In the following discussion we define electrical power flowing in and mechanical power flowing out of the dynamometer machine both as positive.

The first two combinations which can occur have already been mentioned and are intuitive. When the mechanical and electrical powers are both positive, the dynamometer is acting as a motor. In this case P_{in} is the electrical power flowing in and P_{out} is the

mechanical power flowing out. When the mechanical and electrical powers are both negative, the dynamometer is acting as a generator. In this case P_{in} is the mechanical power flowing in and P_{out} is the electrical power flowing out.

The third combination arises when the mechanical power is negative and the electrical power is positive. This occurs at low speed but high torque when insufficient mechanical power flows in to exceed the machine losses at that torque level. Consequently additional electrical power flows into the machine. In this case the power flowing out, P_{out} is zero and power flowing in, P_{in} is the sum of the electrical and mechanical power.

The final combination occurs when the mechanical power is positive and electrical power is negative. This unlikely condition might occur when the dynamometer rotor must be decelerated extremely rapidly. A plausible scenario would be simulating wheel lockup under regeneration. In this case instantaneous efficiency is undefined as P_{in} is zero and P_{out} is the sum of the mechanical and electrical power.

5 SIMULATION OF THE EFFICIENCY MODELS

The DC machine simulated as the regenerative dynamometer was a separately excited Macfarlane 50kW DC machine. The armature of the dynamometer is rated at 440V, 114A with a resistance of 0.133Ω. The field winding of the dynamometer is rated at 205V, 3.68A with a resistance of 55.76 Ω.

The two models presented in Sections 3.1and 3.2 were simulated using a combination of Matlab and Simulink that incorporated the theory in Sections 3.3 and 3.5. M-file script incorporating the theory in Section 4 was used to calculate the cycle and instantaneous efficiencies. The MUT was driven using four drive cycles: Air Resources Board No.2 (ARB02), Urban Dynamometer drive (UDDS), Highway Fuel Efficiency Test (HYFET) and New York City Cycle (NYCC).

The lower section of Figure 5 shows a section of the ARB02 drive cycle that was used to obtain the rigid mass dynamometer model's mechanical and electrical power shown in the upper section of Figure 5. The efficiency was then calculated for the section of the ARB02 drive cycle and the locus it traces through the mechanical and electrical power plane plotted in Figure 6. The interesting points to note in the locus plot is that under heavy vehicle acceleration and deceleration the efficiency is poor for the dynamometer as the resistive losses are exceptionally high. Furthermore as the dynamometer changes from generator to motor the efficiency goes to zero as it transits the negative mechanical power and positive electrical power quadrant.

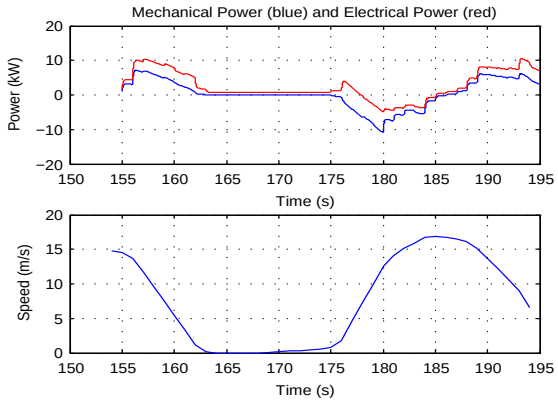

Figure 5: (Upper) Mechanical Power (blue) and Electrical Power minus Field loss (red). (Lower) Section of ARB02 drive cycle.

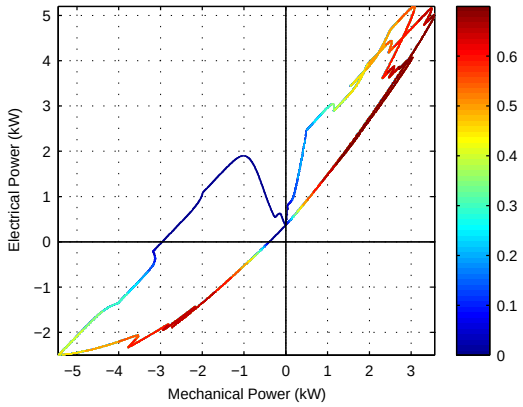

Figure 6: Efficiency locus of the regenerative dynamometer.

The cycle efficiencies for the regenerative dynamometer's emulation of the road load during the four drive cycles are given in Table 2. Comparing the cycle efficiencies for the regenerative dynamometer one can see that the constant field loss of 0.75 kW has a significant impact on the energy returned to the MUT or batteries. If the power consumption of the field could be reduced the more attractive no field loss cycle efficiencies could be approached.

Drive cycle	Cycle Efficiency			
	Rigid mass Model		Spring-damper Model	
	Field loss	No field loss	Field loss	No field loss
ARB02	62.362	79.644	61.021	77.661
UDDS	35.512	71.759	34.222	68.612
HYFET	56.300	90.255	55.853	89.079
NYCC	22.007	53.999	21.098	50.039

Table 2: Cycle Efficiencies

The instantaneous efficiency for the regenerative dynamometer over the 4 drive cycles was correlated against dynamometer speed and torque. The instantaneous efficiency of the dynamometer under road load emulation was interpolated and plotted in figure 7. The steady state instantaneous efficiency was then calculated and plotted in figure 8. In comparison the surface in figure 7 differs dramatically

from the surface in figure 8 and demonstrates the need for dynamic emulation. Traditionally the efficiency data given in figure 8 would have been used for efficiency calculations, differing dramatically from the efficiency of the dynamic application.

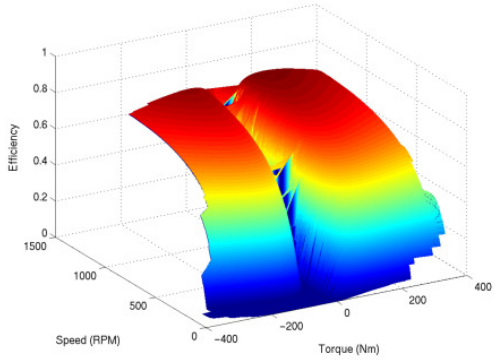

Figure 7: Instantaneous efficiency under dynamic road load emulation

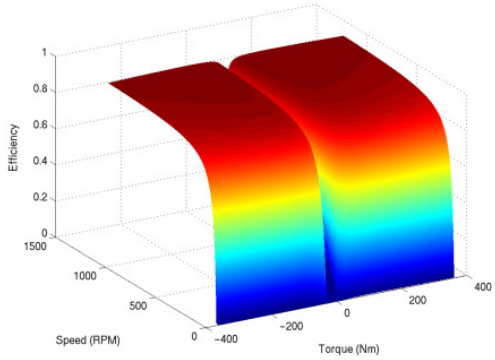

Figure 8: Steady state instantaneous efficiency

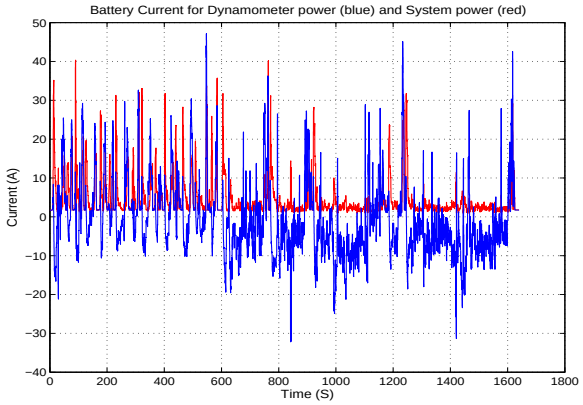

Figure 9: Grid current for the dynamometer (blue) and the MUT and dynamometer system (red)

The final component of the simulation was to see if grid connectivity was a rational option. Figure 9 shows the ARB02 cycle grid current for two cases: the dynamometer being powered by the grid and the MUT and dynamometer system being powered by the grid. The grid connectivity for the dynamometer alone will require a complex inverter/converter or negative energy dissipation technique to be implemented. The MUT and dynamometer system is a more attractive for grid connection as there is no negative power dissipation required and a simple converter topology can be realized to the shared dc bus.

6 CONCLUSIONS

Simulations show the current regenerative dynamometer topology is significantly less efficient under the dynamic conditions of road load testing. These inefficiencies can be reduced significantly by controlling the field current consequently reducing the field losses. A permanent magnet field would eliminate field losses entirely.

The grid connectivity for the regenerative dynamometer is simplified if the MUT and the dynamometer are jointly connected to the grid. A still more robust design would be to power either the dynamometer or the MUT and dynamometer system from a high voltage battery pack that is charged from the grid during the motor testing. This will reduce the complexity of the converter design, increase the life of the battery pack and fully utilise the regenerative feature of the dynamometer.

The simulation results presented are anticipated to be experimentally validated using the DC machine described in Section 5 and the Ultracommuter wheel motor.

7 REFERENCES

[1] C. C. Chan and K. T. Chau, *Modern Electric Vehicle Technology*: Oxford Press, 2001.

[2] M. C. Greaves, A. G. Simpson, B. D. Guymer, G. R. Walker, and D. A. Finn, "Ironless wheel motor for a direct drive vehicle application," presented at Australasian Universities Power Engineering Conference, AUPEC2003, Christchurch, NZ, 2003.

[3] J. M. Miller, *Propulsion Systems for Hybrid Vehicles*: IEE Publishing, 2003.

[4] A. G. Simpson and G. R. Walker, "A Parametric Analysis Technique for Design of Fuel Cell and Hybrid-Electric Vehicles," presented at 2003 SAE International Future Transportation Technology Conference, Costa Mesa, CA, USA, 2003.

[5] L. Weng, G. Walker, Z. Dong, D. Finn, and A. Simpson, "Design of a Regenerative Road Load Simulator," presented at Fifth International Conference on Power Electronics and Drive Systems PEDS 2003, Singapore, 2003.

[6] S. A. Nasar and L. E. Unnewehr, *Electromechanics and Electric Machines*, Second ed. United States of America: John Wiley &Sons, Inc., 1983.

[7] P. A. Tipler, *Physics for Scientists and Engineers*. New York: W.H. Freeman and company, 1999.

[8] I. A. Stringer, "A Regenerative Road Load Simulator," in *Department of Mechanical Engineering*. Brisbane: University of Queensland, 1983.

[9] G. R. Slemon and A. Straughen, *Electric Machines*. USA: Addison-Wesley Publishing Company, Inc, 1980.

[10] Powerx, " PM300RSD060 Intellimod™ datasheet."

[11] L. E. Unnewehr and R. Freedman, "A Comparative Evaluation of Battery Models for Electric Vehicle Simulation," presented at IAS Annual Meeting (IEEE Industry Application Society), Cleveland, OH, USA, 1979.

[12] L. E. Unnewehr and S. A. Nasar, *Electric Vehicle Technology*: John Wiley & Sons, 1982.